AIChE

Behavioral Patterns of Drop Impingement onto Rigid Substrates with a Wide Range of Wettability and Different Surface Temperatures

Xiying Li, Xuehu Ma, and Zhong Lan
Institute of Chemical Engineering, Dalian University of Technology, Dalian 116012, China

DOI 10.1002/aic.11849
Published online June 23, 2009 in Wiley InterScience (www.interscience.wiley.com).

This article concerns behavioral patterns of droplet impingement onto solid substrates covering a wide range of wettability from hydrophilic to superhydrophobic surfaces heated at different temperatures. For droplet impingement onto partial hydrophobic surfaces (mirror-polished Cu substrate), the maximum heights of receding droplet undergoing a consecutive increment with surface temperature can be explained taking account of Marangoni flow. Also, the relation to predict the increment of droplet heights with surface temperature was manifested in the light of lubrication approximation combined with energy conservation. However, this relation is only valid for droplet impacts onto partial hydrophobic surface, because the recoiling droplet height was observed to be independent of surface temperature for both hydrophilic and superhydrophobic targets. This phenomenon was attributed to inherent wettability accompanying larger contact angle hysteresis for the hydrophilic substrate and to the presence of an adiabatic gas layer between the composite surface and impacting droplet, for the superhydrophobic target. © 2009 American Institute of Chemical Engineers *AIChE J,* 55: 1983–1992, 2009

Keywords: droplet impact, lubrication approximation, Marangoni flow, wettability

Introduction

Drop impact on dry solid substrates is a pivotal issue not only because of its relevance to a variety of practical applications, such as ink-jet printing, spray cooling, solidification of steel, internal combustion engines, pesticide spraying, spray painting and coating, and so on, but also because of the complexity of the physical, chemical, and thermal processes involved in droplet/wall interactions. Among these, the physical and fluid hydrodynamic mechanisms involved in finger instability threshold are still an open problem, as well as nonintegrated shear-stress singularity in the vicinity of moving contact line and the modeling of dynamic contact angle, which is applied to get an accurate description of the motion of the triple contact line. The dynamic behavior of an impinging droplet is susceptible to the acting forces, mainly involving inertial, surface tension, and viscous forces, which are the sculptors in liquid drops, and the fashion pertaining to spreading/recoiling, especially for splashing, is exquisite, reminiscent of artistic picture. However, the behaviors of delicate pattern related to drop impingement are ephemeral, such that the study on drop impact often demands the use of high-speed cameras. Various scenarios, mainly including deposition, prompt splash, corona splash, receding break-up, partial rebound, and complete rebound[1] captured by the high-speed camera, can emblem the features of drop impingement onto dry solid surface. The outcomes of drop impact are influenced by many factors including size and speed of the impacting droplet, physical properties of liquid,[2] surface topography[3–6] and wettability,[7–9] addition of polymer additives,[10–12] and surrounding air pressure.[13]

When liquid droplet impacts on hot surface, behavioral patterns of impinging droplet are subject to heat transfer between impacting substrate and liquid droplet.[14–19] In the

Correspondence concerning this article should be addressed to X. Ma at xuehuma@dlut.edu.cn

course of drop impact, heat flux can be determined by experimental study[20–22] or numerical simulation.[23–27] Empirical relations of heat flux can effectively evaluate heat transfer during the whole process of droplet impact, but they cannot respond to different temporal behaviors of heat transfer in relation to droplet impact. Numerical simulation, primarily based on VOF algorithm, can delineate droplet deformation, pressure, and velocity field, as well as the temperature field of liquid drop and the heating surface, irrespective of neglecting some minor factors. While specially referring to very low Weber in the order of 0.01, theoretical study[28–30] on droplet deformation was carried out: in the case of impingement on superhydrophobic substrates, omitting the effects of contact angle hysteresis and viscous energy dissipation for short contact time 2 ms, the value of restitution coefficient $\varepsilon(\varepsilon = |V'/V|)$, where V and V' are the velocities before and after the impact, is constant at 0.91, and the maximal deformation is proportional to the impact velocity while the contact time is independent of the impact velocity. Also, several equations, derived primarily by energy conservation, are available to estimate the maximum spreading diameter of impacting droplet.[15,31–33] Furthermore, based on the mass and momentum balance in the liquid rim, Roisman et al.[34] established a strictly theoretical model accounting for the whole process of drop impact on rigid substrates, regardless of substitution of average contact angle for dynamic contact angle and simplification of real flow as creeping flow, which can predict the evolution of drop diameter within a wide range of experimental parameters. In addition, when the size of impacting droplet is reduced to the order of micrometer featuring ink-jet print,[35–37] some models, especially for low Weber number, are no longer valid.

According to the review of aforementioned articles, even though detailed and theoretical analysis together with a lot of experiments concerning drop deformation after impacting are presented, the study on the dependence of the height variations of rebounding drops on heat transfer between the droplet and hot surface is deficient as yet. However, for many practical applications, involving spray cooling and ink-jet print, the changes of impacting substrates temperature play an important role in the behavioral pattern of impacting droplets. This article highlights the attempt to explore the behavioral patterns of drop impingement onto solid substrates within a wide range of wettability, from hydrophilic to superhydrophobic surfaces, heated at different temperatures. For partial hydrophobic surfaces (mirror-polished Cu surface), the results demonstrated that the maximum heights of droplet recoiling underwent a consecutive increment with the impacting surface temperature, which can be explained taking into account Marangoni flow resulting from the surface tension gradients of liquid adjacent to hot solid surface. Also, the relation to predict the increment of droplet heights with surface temperature was manifested in the light of lubrication approximation combined with energy conservation. However, this relation is only valid for droplet impact onto the partial hydrophobic surface, because the recoiling droplet height was observed to be independent of surface temperature for both hydrophilic and superhydrophobic targets. This phenomenon was attributed to the inherent wettability accompanying a larger contact angle hysteresis for the hydrophilic substrate and to the presence of an adiabatic gas layer between the composite surface and impacting droplet, for the superhydrophobic target.

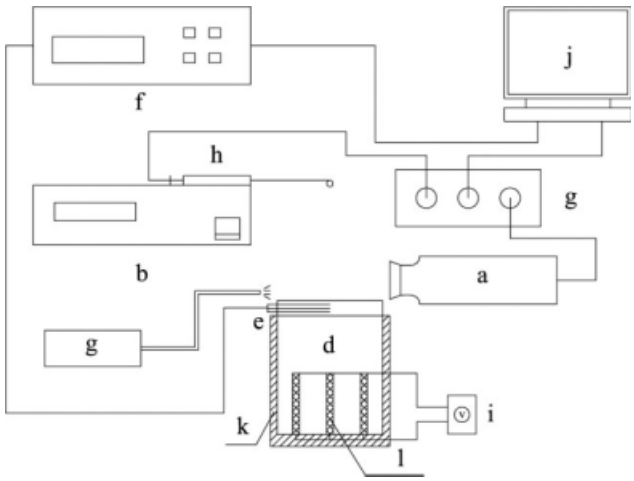

Figure 1. The experimental set-up.

(a) Coupled-charge devise (CCD); (b) electronic infusion pump; (c) light source; (d) impacting substrate; (e) thermocouples; (f) digital meter; (g) trigger; (h) syringe and hypodermic needle; (i) voltage converter; (j) computer; (k) heat insulation; (l) cartridge heater.

Experimental

Apparatus and implementation

The experimental set-up is shown in Figure 1. Water drops with diameter of 2.7 ± 0.03 mm were generated using a syringe with hypodermic needle driven by a pump, and subsequently impacted onto various horizontal surfaces, mainly involving hydrophilic, partial hydrophobic, and superhydrophobic surfaces. The heated block was a vertical copper cylinder having 25 mm diameter and 45 mm height, whose top surface was a mirror-polished, horizontal heat transfer surface where droplet impact happened. On the same mirror-polished Cu substrate, the wetting and superhydrophobic surfaces, respectively, were fabricated by sol–gel[38] and dislocation-selective chemical etching.[39] The hydrophilic surface was fabricated by immersion of the mirror-polished Cu substrate into hydrolyzed $Si(OC_2H_5)_4$ (TEOS) solution and subsequent heat treatment. The superhydrophobic surface was prepared by the combination of chemical hydrophobes (fluoroalkylsilane, tridecafluorooctyltriethoxysilane, $C_8F_{13}H_4Si(OCH_2CH_3)_3$) and surface roughening method (chemical etching). The surface was heated by cartridge heaters (500 W maximum power) and the extrapolated surface temperatures were controlled within $\pm 1^{\circ}C$ by using heat insulation materials (mineral wool) at the bottom and around the lateral wall of the Cu cylinder if the voltage converter was adjusted at the given value. The test surface temperature was measured by extrapolating the measurements of three K-type thermocouples with the equal interval of 3 mm successively. The uppermost thermocouple was located 1 mm below the center of the upper surface. The voltage signals of three thermocouples were collected by a digital meter (Agilent 34970) and transmitted to a computer. The coupled-charged devise (Photron, Fastcam Apx-Rs

Table 1. Dimensionless Parameters Covered in the Experiments

Dimensionless Parameters	Expression	Hydrophilic and Mirror-Polished Cu Substrate	Superhydrophobic Surface
We	$\rho U_0^2 D_0/\sigma$	22	8.1
Re	$\rho U_0 D_0/\mu$	2080	1261
Oh	$\mu/\sqrt{\rho D_0 \sigma}$	0.002	0.002
Ca	$\mu U_0/\sigma$	0.01	0.006

which is mounted on a long distance microscope, Hirox, OL-35, Japan) was applied to record the transient features of drop impact and the synchronization of the recording events and the detachment of droplet off the needle tip was validated by the trigger. The magnification was adjusted to ensure that the image could include the maximum spreading diameter and height of the droplet. Additionally, a fiber optic solarc light source (Welch Allyn Inc., USA) was used to backlight the droplet impact events.

Image processing and data acquisition

In the scenario of drop impingement onto hydrophilic or partial hydrophobic surface, high speed digital motion pictures of droplet impact were recorded at 3000 frames per second with 1024 × 1024 pixel resolution, while 5000 frames per second with 1024 × 512 pixel resolution was used to capture the features of droplet collision with superhydrophobic surface thanks to faster variations of contact radius and receding height, resulting from droplet impact onto this substrate, when compared with others. Measurements on the contact radius, receding droplet height, as well as dynamic contact angle, were performed directly from the images using a calibration scale with a characteristic length of 1 mm subdivided into 100 partitions and image processing software (Image-Pro Plus). The initial speed of impacting droplet can be determined by the distance and the time interval of the two successive frames captured immediately before droplet impacting on the substrate. Accordingly, the spatial resolution is determined in the order of 10 μm/pixel and U_0 accuracy is 0.03 m/s in our experiments. Although the temporal and spatial resolutions are precise enough to get reliable information from the series of successive pictures, the reproducibility of the results is intrinsically sensitive to impacting surface wettability which is susceptible to dust contamination present in ambient atmosphere. Thereby, the results presented in this article are representative of the outcome of five repeated occurrences. Additionally, great care should be taken to maintain experimental surface free of contamination. The samples were washed by ultrasonication in distilled water after treatment with acetone. The experimental parameters such as Reynold (*Re*), Weber (*We*), Ohnesorge (*Oh*), Capillary (*Ca*) numbers, and surface wettability characterized by θ_e, θ_a, θ_r, which indicate equilibrium, quasi-static advancing, and receding contact angles, respectively, were measured by a contact angle meter (Contact Angle System OCA20, Dataphysics, Germany) at room temperature, and are shown in Tables 1 and 2, respectively. Equilibrium contact angle can be measured by placing a water droplet of 3 μl on the substrate, and the advancing/receding angle can be obtained by the addition/removal of liquid at the rate of 0.3 μl/s.

Table 2. Contact Angles on the Impacting Substrates

Impacting Surfaces	θ_e (°)	θ_a (°)	θ_r (°)	$\theta_a - \theta_r$ (°)
Mirror-polished Cu	97	103	72	31
SiO_2 surface	52	55	21	34
Superhydrophobic	170	168	166	2

Results and Discussion

Behavioral patterns of droplet impact on mirror-polished Cu substrate

Considering the regimes of *We* and *Oh* relevant to our experiments, the features of droplet impact can be categorized as IC-CI region (where I and C denote inertia and capillarity, respectively) whereby the drop dynamics is governed by a competition between inertia and capillarity both for the spreading and the retraction with reference to the Phase diagram[40] in Figure 2. Sequential images of water droplets impingement on mirror-polished Cu substrates heated at different temperatures are shown in Figure 3. As the droplet contacts the substrate, the liquid film rapidly propagates outward, in the radial direction, under the action of inertia. During the initial stage of spreading, the droplet changes its shape from a spherical shape to a disc-like profile. Presence of pyramidal structure with capillary waves[41] propagating from the bottom to the top of the droplet was observed on the liquid/gas interface in the initial spreading phase. At the later stages of spreading, kinematic energy is stored into surface energy and is partly dissipated by viscous friction irreversibly; thereby the propagating velocity of the contact line slows down. Thereafter, triple line is pinned for a short while due to contact angle hysteresis and then moves adversely at a low speed driven by surface tension and capillary force. The contour of the recoiling droplets is ranged from gable to dumb-bell shape. Then, the liquid becomes thinner and thinner at the neck whereby pinching-off happens once the surface temperature reaches 100°C. In our experiment, the maximum value of surface temperature was

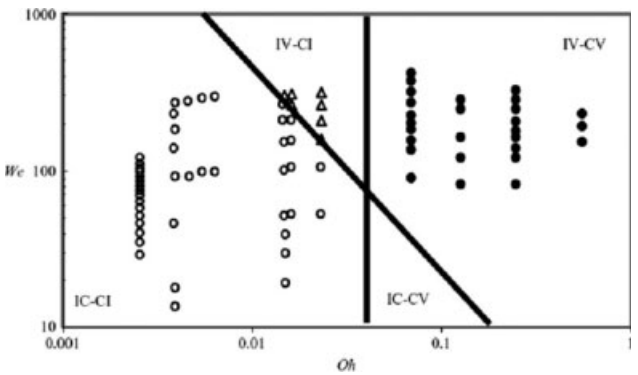

Figure 2. Overview of experiments performed in Bartolo[40] diagram, phase diagram in the (We, Oh) plane for the impact and retraction dynamics of droplets, where I, C, and V represent inertial, capillarity, and viscous, respectively.

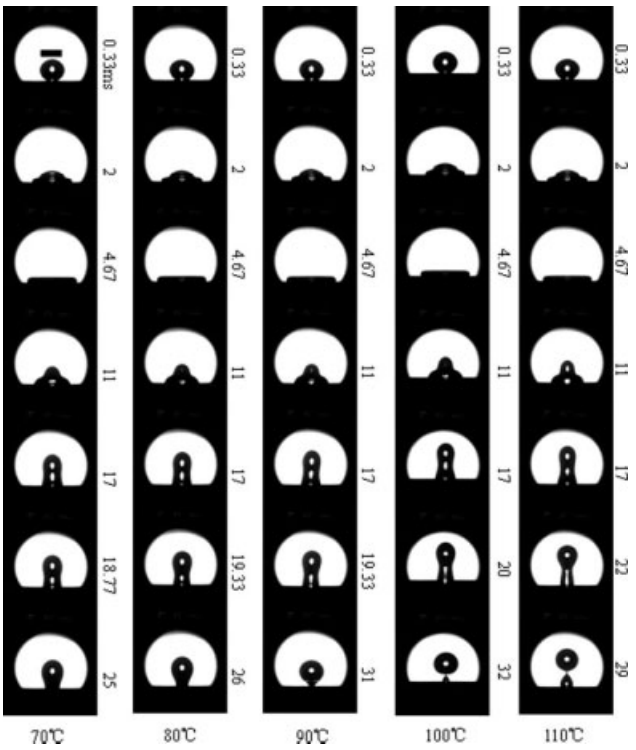

Figure 3. Behavioral patterns of drop impingement onto mirror-polished Cu substrate subject to heating up to different surface temperatures.

The scale bar represents 2 mm.

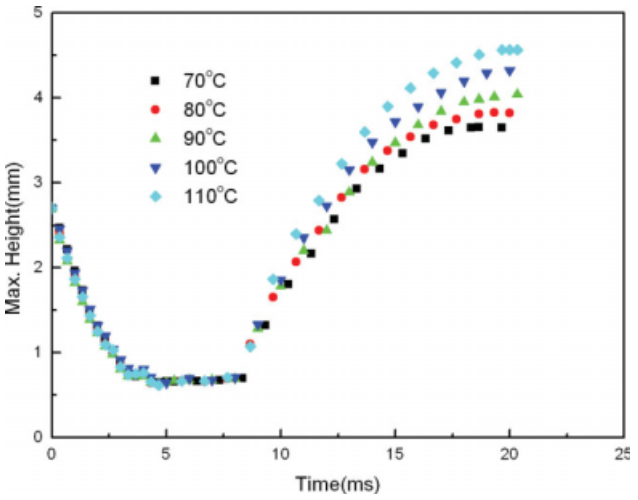

Figure 4. Temporal evolution of the droplet height after impact on mirror-polished Cu surfaces, heated at different temperatures.

[Color figure can be viewed in the online issue, which is available at www.interscience.wiley.com.]

set at 110°C to avoid the implications of secondary drop resulting from nucleation boiling (occurring around the periphery of the wetted spot in the receding stage when the surface temperature is above 120°C in our experiments). These images in Figure 3 show that the height of the receding droplet increases stepwise and suggest that the maximum droplet height depends on the surface temperature. This is further confirmed by the quantitative results, shown in Figure 4, which depict the temporal evolution of heights of the impacting droplets. The phenomena of the recoiling stage are very similar to the shrinkage characteristics of heated falling liquid films.[42] In the same way, the dependence of height changes of recoiling droplet on surface temperatures can be ascribed to Marangoni flow driven by surface tension gradients triggered by surface temperature gradients in liquid film affiliated to the substrate where heat transfer occurs. Provided that the temperature field of the impacting droplet can be achieved, attendant surface tension gradients, together with continuity and momentum equations, should be used to account for the additional height changes of receding droplet. In fact, it is a substantially difficult task to achieve the temperature field of an impacting droplet due to its intrinsic complexity arising from the coupling of free surface flow and heat transfer. Consequently, it is infeasible to achieve analytical expressions for the temperature field of impacting droplet with the exception of numerical simulation.[23,25,27] Marangoni number can be estimated with reference to the simulation results of Pasandideh-Fard et al.[23] as shown in Figure 5. The Marangoni number $Ma = \gamma(\Delta T_{\delta_T})(\delta_T)/\mu\alpha =$ 1740 is considerably larger than $M_{cr} = 80$ corresponding to the onset of the fluid motion on a heated flat wall,[43] where $\gamma = d\sigma/dT$ is temperature coefficient of surface tension which is a constant for a specific liquid, ΔT_{δ_T} represents the temperature difference in the thermal boundary layer, δ_T indicates the thickness of thermal boundary layer, μ and α denote viscosity and thermal diffusivity of liquid, respectively, σ signifies liquid surface tension, T is temperature. Additional flow resulting from Marangoni effect can be tackled exceptionally when selecting the frame of reference moving with the "base flow" referred to as droplet impact devoid of heat transfer. As a result, additional flow can be essentially analogous to liquid film flow upward on an inclined plate with a temperature distribution descending from bottom to top as shown in Figure 6, whose slope can be determined by the examination of the dynamic contact angle in the receding stage. The dynamic contact angles in the receding phase were demonstrated in Figure 7. It was demonstrated that receding contact angles mostly underwent the oscillation of $\pm 10°$ around the value of 70° which was approximately equal to the value of θ_r (72°) measured at ambient temperature. So, the receding contact angle at ambient temperature is considered as the slope of the inclined plate. Also, the receding contact angles are insensitive to the substrate temperature in our experiments. The thickness of

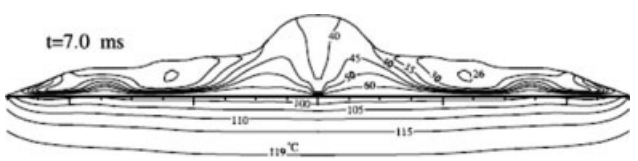

Figure 5. Simulation result by Pasandideh-Fard et al.[23]

Temperature distribution in a 2-mm water droplet at 25°C impacting with the velocity of 1.3 m/s on a stainless steel surface at the temperature of 120°C.

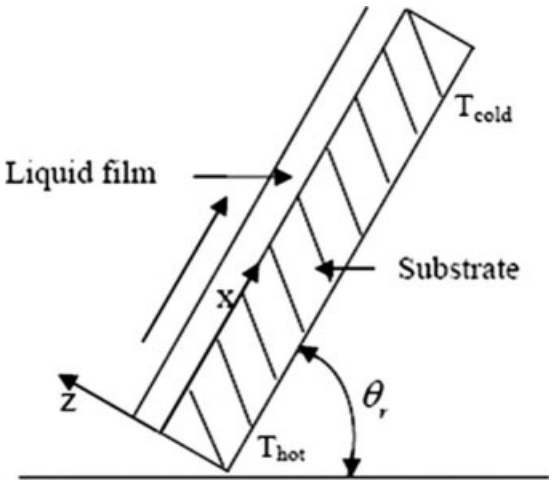

Figure 6. Schematic of liquid film flowing upward under the action of surface temperature gradient on an inclined plate.

the liquid film δ_0 under the action of Marangoni flow featured boundary layer and can be evaluated by the Eq. 1,[31]

$$\delta_0 = 2D_0/Re^{0.5}, \tag{1}$$

$$Re = \rho D_0 U_0/\mu, \tag{2}$$

where ρ represents the liquid density, D_0 and U_0 indicate, respectively, the initial diameter and velocity of droplet while just contacting the substrate. The resulting thickness of liquid film is in the order of 10^{-4} m. Based on the fact that the ratio of liquid film thickness to receding droplet height $\delta_0/h \sim 10^{-2}$ is far below unity, it is within the framework of lubrication approximation[44] applied to circumvent liquid film flow driven by surface tension gradient. For receding stage, the liquid film is nearly smooth such that capillary pressure, pertaining to surface tension and curvature, is negligible. Accordingly, the Navier-Stokes equation[45,46] of the motion of receding droplet is written in the lubrication approximation:

$$\mu\frac{\partial^2 u}{\partial z^2} = \rho g \sin\theta_r, \tag{3}$$

where u represents the velocity in the flow direction x, z perpendicular to the flow direction, g is gravitation acceleration. The average temperature rise in the impacting liquid droplet can be estimated as less than 10° with surface temperature up to 110° on the assumption that heat flux by conduction from Cu substrate can be completely transferred to liquid droplet. Considering a very limited scope of surface temperature covering in our experiments, it is rational to assume the density and viscosity of liquid as constants independent of surface temperature. Similar approximation of the density and viscosity of liquid can be found in Refs. 45 and 46. The lubrication Eq. 3 can be solved subject to the no-slip boundary condition at the solid surface

$$u\big|_{z=0} = 0, \tag{4}$$

and shear stress, $\tau = \gamma(dT/dx)$, at the air-liquid interface

$$\mu\frac{du}{dz}\bigg|_{z=\delta_0} = \tau = \gamma\frac{dT}{dx}, \tag{5}$$

Considering the short time interval of about 14 ms from the receding start to the occurrence of maximum receding height, the temperature gradient dT/dx in the direction of liquid film flow can be substituted for $(\Delta T_{\delta_T}/\delta_T)\sin\theta_r$ which represents the temperature gradient component in the thermal boundary layer and keeps constant.

$$dT/dx = (\Delta T_{\delta_T}/\Delta_T)\sin\theta_r. \tag{6}$$

In fact, this assumption somewhat overestimates the temperature gradient dT/dx in that once Marangoni flow starts the temperature gradient is redistributed. Also, the thickness of the thermal boundary layer δ_T can be given in Eq. 7.[23]

$$\delta_T = 2D_0/Re^{0.5}Pr^{0.4}. \tag{7}$$

with

$$Pr = c_p\mu/k, \tag{8}$$

where c_p indicates the specific heat, k designates the thermal conduction. By solving lubrication Eq. 3 in consideration of Eqs. 4, 5, and 6, the resulting velocity distribution perpendicular to the inclined plate can be given:

$$u = \frac{\rho g \sin\theta_r}{2\mu}y^2 + \left(\gamma\frac{\Delta T_{\delta_T}}{\delta_T} - \delta_0\rho g\right)\frac{y}{\mu}\sin\theta_r. \tag{9}$$

Here, some of the terms in Eq. 9 can be discarded by order-of-magnitude argument. These variables can be estimated as in our experiments: $\gamma \sim O(10^{-4}\text{kg°C}^{-1}\text{s}^{-2})$ for water, $\Delta T_{\delta_T} \sim O(10°\text{C})$, $\delta_T \sim O(10^{-5}\text{m})$, $\delta_0 \sim O(10^{-4}\text{m})$, thereby getting the outcome of

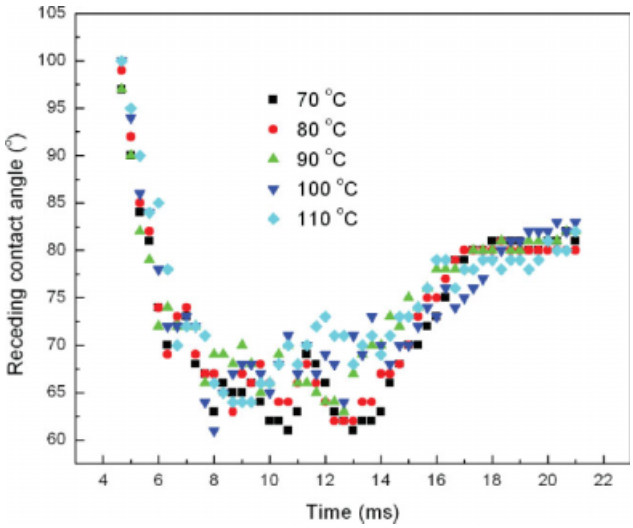

Figure 7. Temporal evolution of receding contact angle after occurrence of droplet retraction.

[Color figure can be viewed in the online issue, which is available at www.interscience.wiley.com.]

$\gamma \frac{\Delta T_{\delta_T}}{\delta_T} \sim O(10^2 \mathrm{kgm^{-1}s^{-2}}) >> \delta_0 \rho g \sim O(1\ \mathrm{kgm^{-1}s^{-2}})$ which corroborates that the effect of gravitation is negligible for the thin liquid film flow in comparison with the variation of liquid surface tension. In fact, the Bond number with the expression for $Bo = \rho g \delta_0^2/\sigma$ is in the order of 10^{-2}, which also substantiate the validity of the negligence of gravitation effect. Accordingly, the velocity u at the air–liquid interface reduces to

$$u\big|_{z=\delta_0} = \frac{\gamma}{\mu}\frac{\delta_0}{\delta_T}(\Delta T_{\delta_T})\sin\theta_r. \tag{10}$$

The temperature difference in thermal boundary layer can be estimated as the function of initial temperatures in liquid droplet and impacting substrate if all the energy entering from the substrate is used to heat the liquid in thermal boundary layer. The equations can be given as follows:

$$\int_{r_1}^{r_2} c_p(\Delta T_{\delta_T}) d\left(\pi \rho r^2 \delta_T\right) = \int_{t_1}^{t_2} k \frac{T_{s0} - T_{d0}}{\delta_T} \pi r^2 dt, \tag{11}$$

where r is the time-dependent radius of wetted area. Concerning a lack of sufficient information about the dynamic of contact line and temperature field in liquid and substrate, after integration of Eq. 11, the Eq. 12 can be given explicitly by the introduction of two numerical prefactors ε and β which should be related to the temporal evolution of contact diameter of wetted area.

$$\pi \rho (\varepsilon D_0)^2 \delta_T c_p(\Delta T_{\delta_T}) = k \frac{(T_{s0} - T_{d0})}{\delta_T} \pi (\beta D_0)^2 (\Delta t), \tag{12}$$

where Δt represents the elapsed time after impacting. Consequently, the difference of temperature in thermal boundary layer can be given:

$$\Delta T_{\delta_T} = \left(\frac{\beta}{\varepsilon}\right)^2 \alpha \frac{(T_{s0} - T_{d0})(\Delta t)}{\delta_T^2}. \tag{13}$$

In consideration of Eq. 13, Eq. 10 can be rewritten as:

$$u|_{z=\delta_0} = \left(\frac{\beta}{\varepsilon}\right)^2 \frac{1}{Pr}\frac{\gamma}{\rho}\frac{\delta_0}{\delta_T^3}(T_{s0} - T_{d0})(\Delta t)\sin\theta_r. \tag{14}$$

Furthermore, the addition height arising from Marangoni flow can be expressed as:

$$\begin{aligned} h &= (\Delta t')\sin\theta_r u\big|_{z=\delta_0} \\ &= \left(\frac{\beta}{\varepsilon}\right)^2 \frac{1}{Pr}\frac{\gamma}{\rho}\frac{\delta_0}{\delta_T^3}(\sin\theta_r)^2 (T_{s0} - T_{d0})(\Delta t)(\Delta t'), \end{aligned} \tag{15}$$

where $\Delta t'$ is the duration in which Marangoni flow acts. Here, we argue that Marangoni flow occurs when droplet retraction starts. Considering slow height increment of recoiling droplet, the receding stage can also be interpreted in terms of quasi-steady approximation. In this regime, the driving force of surface tension gradient resulting from temperature gradient is in equilibrium with viscous force. As a consequence, the following correlation can be achieved dimensionally:

Table 3. Comparison of the Experimental Data and Correlation Results

Ratio (Different Temperature at t = 19 ms)	From Experimental Data	From Correlation 19
$h_{80°C}/h_{70°C}$	1.12	1.20
$h_{90°C}/h_{70°C}$	1.32	1.40
$h_{100°C}/h_{70°C}$	1.50	1.60
$h_{110°C}/h_{70°C}$	1.67	1.80
Ratio (At Different Time for 100°C)	**From Experimental Data**	**From Correlation 20**
$h_{100°C(15ms)}/h_{100°C(14ms)}$	1.20	1.19
$h_{100°C(16ms)}/h_{100°C(14ms)}$	1.36	1.39
$h_{100°C(17ms)}/h_{100°C(14ms)}$	1.51	1.60
$h_{100°C(18ms)}/h_{100°C(14ms)}$	1.64	1.84
$h_{100°C(19ms)}/h_{100°C(14ms)}$	1.73	2.08

$$\gamma \frac{dT}{dx} \approx \mu \frac{u}{\delta_0}. \tag{16}$$

Similarly, we can get the same result as obtained by solving lubrication equation.

$$u \approx \frac{\gamma}{\mu}\frac{\delta_0}{\delta_T}(\Delta T_{\delta_T})\sin\theta_r \tag{17}$$

Although it is impossible to determine the real value of height variation, the ratio of height variation of receding droplet corresponding to different surface temperatures can be obtained on an assumption that the numerical prefactors, β and ε, are all approximately equal:

$$\frac{h_{T_{s1}}}{h_{T_{s2}}} \approx \frac{(T_{s1} - T_{d0})}{(T_{s2} - T_{d0})}\frac{(\Delta t_{T_{s1}}')(\Delta t_{T_{s1}})}{(\Delta t_{T_{s2}}')(\Delta t_{T_{s2}})}, \tag{18}$$

where T_{s1}, T_{s2} represent two different initial surface temperatures. If we take the same elapsed time during the recoiling phase, the Eq. 18 can lead to:

$$\frac{h_{T_{s1}}}{h_{T_{s2}}} \approx \frac{T_{s1} - T_{d0}}{T_{s2} - T_{d0}}. \tag{19}$$

For the same surface temperature, the following correlation can be similarly written as in the form:

$$\frac{h_{T_s,(\Delta t_1)}}{h_{T_s,(\Delta t_2)}} \approx \frac{(\Delta t_1')(\Delta t_1)}{(\Delta t_2')(\Delta t_2)}, \tag{20}$$

$$h_{T_{s1}} = H_{T_{s1}} - H_{T_s0}. \tag{21}$$

The additional heights $h_{T_{s1}}$ can be achieved by the subtraction of receding height $H_{T_{s0}}$ from $H_{T_{s1}}$, which are the heights corresponding to surface temperature T_{s0} and T_{s1}, respectively. T_{s0} represents ambient temperature at which heat transfer does not occur and the value of $H_{T_{s0}}$ can be determined experimentally as 2.40 mm. The comparison of the experimental data and the correlation results is depicted in Table 3. Irrespective of a lack of clear image of flow and heat transfer during droplet impingement, the correlations derived can rationally predict the experimental data in our experiments. It is definite that the

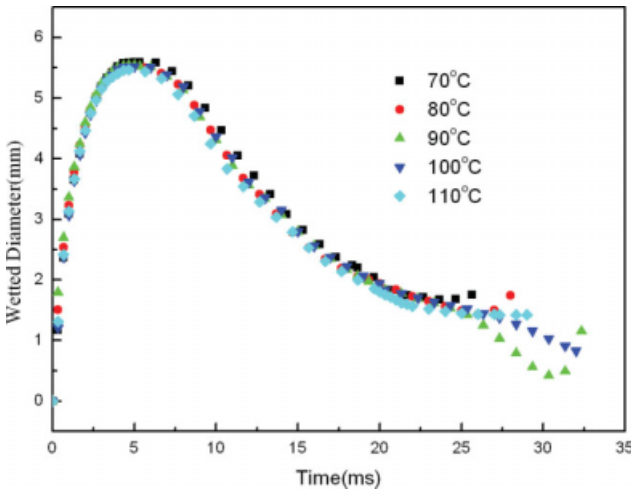

Figure 8. Temporal evolution of the contact diameters after droplet impact on mirror-polished Cu surfaces heated at different temperatures.

[Color figure can be viewed in the online issue, which is available at www.interscience.wiley.com.]

substitution of temperature gradient in thermal boundary for that in the liquid film flow direction leads to overestimation of additional velocity in Eq. 10. Furthermore, the discrepancies partly result from the negligence of the effect of surface temperature on thermal boundary layer and impossibility of precisely determining the incipient time when Marangoni flow comes into effect. It is noticeable that when the receding height approaches the maximum height, the effect of gravitation, having a potential in driving the bulk flow downward, will become considerable and counteract the influence of Marangoni flow to some degree. According to Figure 8, the effect of surface temperature on the motion of moving contact line is not remarkable until pinch-off of liquid droplet occurs. In fact, the dynamics of contact line are influenced by more factors mainly involving uncompensated Young force[47] (resulting from the difference of dynamic contact angle and equilibrium angle), viscous dissipation[48] in the vicinity of the triple line, capillary force as well, which can counterweight the effect of Marangoni flow on the dynamic of contact line. So the behaviors of dynamic of contact line are very similar regardless of different surface temperatures used.

Behavioral patterns of droplet impact on hydrophilic and superhydrophobic substrate

Also of noticeable importance is the influence arising from the acting mechanism of heat transfer occurring on hydrophilic/superhydrophobic surface on droplet impact. As can be seen from Figures 9–12, there are, however, no apparent height variation of receding drop after droplet impinging onto hydrophilic or superhydrophobic surface heated at different temperatures. During the retraction phase on hydrophilic substrates, the contact line is almost quiescent. Considering very low receding velocity of triple line, it seems that the slow contact angle dynamics governs the recoiling evolution. So, it is rational to assume a quasi-static dynamics for the surface shape during receding phase. In this regime, the work done by the capillary force is dissipated by viscous flow close to contact line. Accordingly, the velocity of retracting contact line relevant to dynamic contact angle and liquid property is defined as the correlation[40]:

$$\frac{v_r}{R_{max}} \approx \left(\frac{3}{25}\right)^{1/3} \frac{(1-\cos\theta_r)^{5/3}}{5\ln(\Lambda/\lambda)} \frac{\sigma}{\mu R}, \tag{22}$$

where v_r is retraction velocity of contact line, Λ and λ are macro and micro length, respectively. In fact, the pinning of contact line, due to inherent wettability and larger contact angle hysteresis, considerably influences the flow in the liquid and suppresses Marangoni flow concomitantly, thereby the height variation of receding droplets. As to the receding phase on hydrophilic substrate, the receding contact angle is about 10°–20°, which remarkably weakens the effect of Marangoni flow on additional receding height according to Eq. 15 comparing to partial hydrophobic substrate.

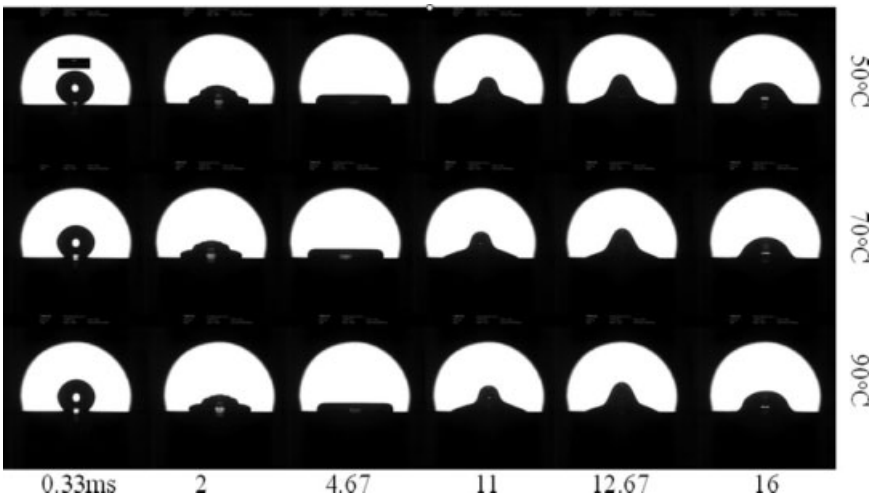

Figure 9. Behavioral patterns of drop impingement onto SiO_2 substrates heated at different temperatures.

The scale bar represents 2 mm.

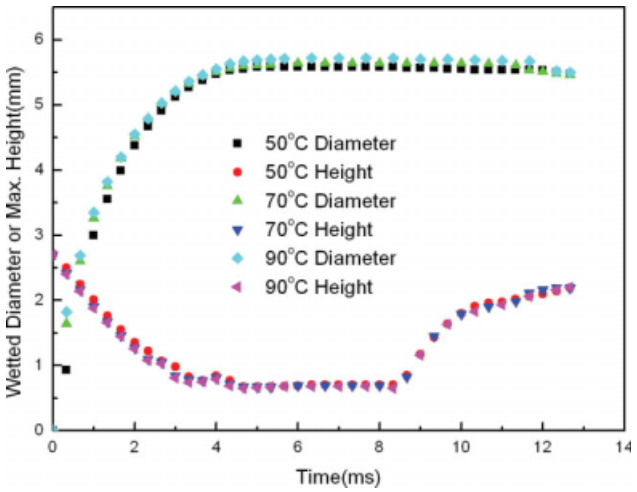

Figure 10. Temporal evolutions of contact diameter and droplet height after drop impingement on SiO_2 surfaces at different temperatures.

[Color figure can be viewed in the online issue, which is available at www.interscience.wiley.com.]

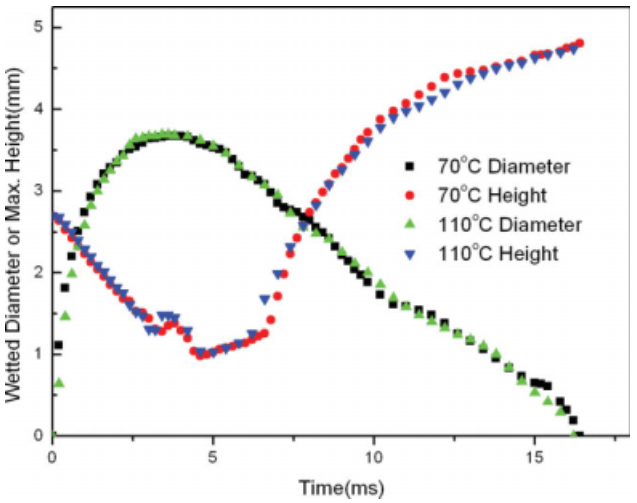

Figure 12. Temporal evolutions of contact diameter and droplet height after drop impact on superhydrophobic surface at different temperatures.

[Color figure can be viewed in the online issue, which is available at www.interscience.wiley.com.]

In addition, the droplet rebounding height is nearly constant for the droplet impact onto superhydrophobic substrate with different temperatures. Comparing to hydrophilic and partly hydrophobic substrates, negligible contact angle hysteresis greatly contributes to the receding movement for the superhydrophobic, such that the impacting droplet can completely rebound off the surface as shown in Figure 11. In view of superhydrophobic surface, the "fakir" state[49] can account for the independence of height variations on the surface temperature. Referring to the superhydrophobic state, the liquid only contacts the solid at the top of the asperities bridging by liquid, accounting for the direct contact area with rigid substrate leading to a fraction of the smooth surface defined as ϕ_s.[50] As a result, the apparent contact angle θ^* of such a "fakir" drop is an average between the angles on the solid (θ), and that on the air (180°), respectively, weighed by the fractions ϕ_s and $1 - \phi_s$. Accordingly, the apparent contact angle in Cassie state can be given by:

$$\cos\theta^* = -1 + \phi_s(\cos\theta + 1). \tag{23}$$

As apparent contact angle $\theta^* = 170°$ and intrinsic contact angle $\theta = 115°$, respectively, corresponding to superhydrophobic surface and fluoroalkylsilane coat on mirror-polished Cu substrate, are known a priori, the value of ϕ_s can be calculated as 2.6%. Also, the impacting velocity $U_0 = 0.47$ m/s is far below the threshold velocity $U^* \approx (\sigma a/\rho l^2)^{1/2} = 12.0$ m/s above which the entrapped air between the liquid droplet and microstructured solid surface is squeezed out and then pinning occurs.[51] The impacting droplet is, therefore, almost "floating" on an air cushion in the course of droplet impact. Herein a and l are the microscopic characteristic sizes of microstructured surface which are determined respectively as 2 μm and 1 μm referring to Ref. 36. Consequently, between the impacting droplet and heating surface the presence of adiabatic air layer eliminates the effective heat transfer to the extent that the effect of the surface temperature on height change of receding droplet is negligible.

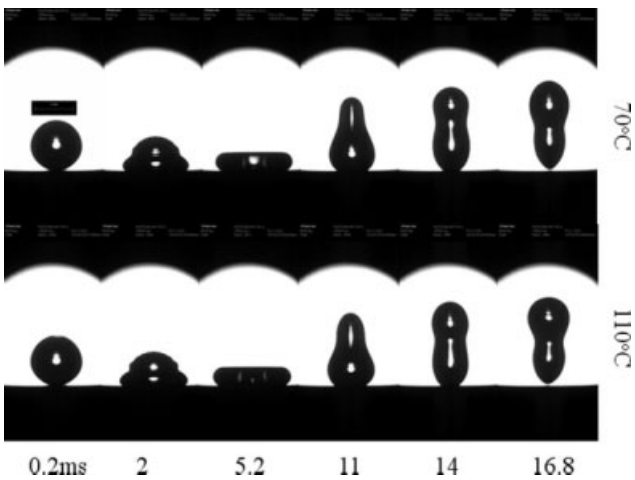

Figure 11. Behavioral patterns of drop impingement onto superhydrophobic substrate heated at different temperatures.

The scale bar represents 2 mm.

Concluding remarks

In this article, the paramount concern is the behavioral patterns of droplet impingement onto solid substrates, covering a wide range of wettability from hydrophilic to superhydrophobic surfaces heated at different temperatures. For droplet impingement onto partial hydrophobic surfaces (mirror-polished Cu substrate), the maximum heights of receding droplet are directly related to the surface temperature. Marangoni flow was used to account for this scenario of droplet impact. Also, a relation, revealing the receding height of

impacting droplet dependent on the surface temperature, was developed in the context of lubrication approximation combined with energy conservation. However, this argument cannot be applied to the events of droplet impact onto hydrophilic or superhydrophobic substrate. Given that the inherent wettability and larger contact angle hysteresis are present on hydrophilic surface, the pinning of contact line remarkably suppresses Marangoni flow. As to superhydrophobic substrate, the acting mechanism of heat transfer is altered due to the presence of adiabatic gas layer between composite surface and liquid droplet such that the heat flux from the substrate no longer enters into the impacting droplet. In the future, more efforts will be devoted to exploring the effects of wettability covering a wider range, contact angle hysteresis and gravitation, on the receding droplet height subject to heat transfer.

Acknowledgements

The authors are grateful to the financial support provided by National Natural Science Foundation of China (Contracts No. 50776012) and Ministry of Education of China (NECT-05-0280).

Notation

a, l = characteristic sizes of microtextured surface
Bo = Bond number ($= \rho g D_0^2/\sigma$)
c_p = specific heat
Ca = capillary number ($= \mu U_0/\sigma$)
D_0 = initial diameter of impacting droplet
D_{max} = maximum spreading diameter
g = gravitation acceleration
h_{T_s} = additional height at specific surface temperature
$h_{T_s,\Delta t}$ = time-dependent additional height at a given surface temperature
H_{T_s} = height of receding droplet at specific surface temperature
H_{T_0} = height of receding droplet at ambient temperature
k = thermal conductivity
m = mass of liquid droplet
Oh = Ohnesorge number ($= \mu/(\rho\sigma D_0)^{0.5}$)
q = heat flux
Pr = Prandtl number ($= c_p\mu/k$)
r = time-dependent radius of wetted area
Re = Reynolds number ($= D_0U_0\rho/\mu$)
R_{max} = maximum spreading radius
Δt = time interval in impacting process
$\Delta t'$ = time interval under the action of Marangoni flow
T_{s0}, T_{d0} = initial temperatures of impacting surface and droplet
ΔT_{max} = maximum temperature rise in liquid droplet
ΔT_{δ_T} = temperature difference in thermal boundary layer
U_0 = initial velocity of impacting droplet
U^* = threshold velocity above which pinning occurs
v_r = retraction velocity of contact line
x,z = coordinates

Greek letters

α = thermal diffusivity
β,ε = numerical prefactors
δ_0 = liquid film thickness
δ_T = thickness of thermal boundary layer
ϕ_s = fraction of the smooth surface
γ = temperature coefficient of surface tension
μ = viscosity
θ_e = equilibrium contact angle
θ_a = advancing contact angle
θ_r = receding contact angle
θ^* = apparent contact angle
θ_0 = intrinsic contact angle
τ = shear stress

Literature Cited

1. Yarin AL. Drop impact dynamics: splashing, spreading, receding, bouncing…. *Annu Rev Fluid Mech*. 2006;38:159–192.
2. Mundo CHR, Sommerfeld M, Tropea C. Droplet-wall collisions: experimental studies of the deformation and breakup process. *Int J Multiphase Flow*. 1995;21:151–173.
3. Xu L. Liquid drop splashing on smooth, rough, and textured surfaces. *Phys Rev E*. 2007;75:056316.
4. Ha EJ, Kim WS, Jeun GD. A study on the impact and solidification of liquid metal droplets during thermal spray deposition onto a substrate with concentric grooves or ridges. *Heat Transfer Eng*. 2006; 27:55–67.
5. Mock U, Michel T, Tropea C, Roisman I, Rühe J. Drop impact on chemically structured arrays. *J Phys: Condens Matter*. 2005;17:595–605.
6. Kannan R, Sivakumar D. Drop impact process on a hydrophobic grooved surface. *Colloids Surf A: Physicochem Eng Aspects*. 2008; 317:694–704.
7. Ukiwe C, Kwok DY. On the maximum spreading diameter of impacting droplets on well-prepared solid surfaces. *Langmuir*. 2005; 21:666–673.
8. Ukiwe C, Mansouri A, Kwok DY. The dynamics of impacting water droplets on alkanethiol self-assembled monolayers with co-adsorbed CH_3 and CO_2H terminal groups. *J Colloid Interface Sci*. 2005;285: 760–768.
9. Chang YW, Ukiwe C, Kwok DY. Chain length effect of alkanethiol self-assembled monolayers on the maximum spreading ratio of impacting water droplets. *Colloids Surf A: Physicochem Eng Aspects*. 2005;260:255–263.
10. Vance B, Bonn D, Martin JY, Vovelle L. Controlling droplet deposition with polymer additives. *Nature*. 2000;405:772–775.
11. Cooper-White JJ, Crooks RC, Chockalingam K, Boger DV. Dynamics of polymer-surfactant complexes: elongational properties and drop impact behavior. *Ind Eng Chem Res*. 2002;41:6443–6459.
12. Bartolo D, Boudaoud A, Narcy G, Bonn D. Dynamics of non-Newtonian droplets. *Phys Rev Lett*. 2007;99:174502.
13. Xu L, Zhang WW, Nagel SR. Drop splashing on a dry smooth surface. *Phys Rev Letters*. 2005;94:184505.
14. Wachters LHJ, Westerling NAJ. The heat transfer from a hot wall to impinging water drops in the spheroidal state. *Chem Eng Sci*. 1966;21:1047–1056.
15. Chandra S, Avedisian CT. On the collision of a droplet with a solid surface. *Proc R Soc Lond Ser A*. 1991;432:13–41.
16. Manzello SL, Yang JC. An experimental study of high Weber number impact of methoxy-nonafluorobutane $C_4F_9OCH_3$ (hfe-7100) and n-heptane droplets on a heated solid surface. *Int J Heat Mass Transfer*. 2002;45:3961–3971.
17. Manzello SL, Yang JC. An experimental investigation of water droplet impingement on a heated wax surface. *Int J Heat Mass Transfer*. 2004;47:1701–1709.
18. Cossali GE, Marengo M, Santini M. Secondary atomisation produced by single drop vertical impacts onto heated surfaces. *Exp Therm Fluid Sci*. 2005;29:937–946.
19. Moita AS, Moreira ALN. Drop impacts onto cold and heated rigid surfaces: morphological comparisons, disintegration limits and secondary atomization. *Int J Heat Fluid Flow*. 2007;28:735–752.
20. Mcginnis FK, Holman JP. Individual droplet heat-transfer rates for splattering on hot surfaces. *Int J Heat Mass Transfer*. 1969;12:95–108.
21. Holman JP, Jenkins PE, Sullivan GG. Experiments on individual droplet heat transfer rates. *Int J Heat Mass Transfer*. 1972;15:1489–1495.
22. Chen JC, Hsu KK. Heat transfer during liquid contact on superheated surfaces. *J Heat Transfer*. 1995;117:693–697.
23. Pasandideh-Fard M, Aziz SD, Chandra S, Mostaghimi J. Cooling effectiveness of a water drop impinging on a hot surface. *Int J Heat Fluid Flow*. 2001;22:201–210.
24. Nishio S, Kim YC. Heat transfer of dilute spray impinging on hot surface (simple model focusing on rebound motion and sensible heat of droplets). *Int J Heat Mass Transfer*. 1998;41:4113–4119.
25. Dalton JEH, David FF. A hydrodynamic and thermodynamic simulation of droplet impacts on hot surfaces, Part II: validation and applications. *Int J Heat Mass Transfer*. 2001;44:2643–2659.
26. Wang W, Hong FJ, Qiu HH, Cheng P. The impact of thermal contact conductance on the spreading and solidification of a droplet on a substrate. *Heat Transfer Eng*. 2006;27:68–80.

27. Ge Y, Fan LS. 3-D modeling of the dynamics and heat transfer characteristics of subcooled droplet impact on a surface with film boiling. *Int J Heat Mass Transfer*. 2006;49:4231–4249.
28. Richard D, Quéré D. Bouncing water drops. *Europhys Lett*. 2000;50: 769–775.
29. Okumura K, Chevy F, Richard D, Quéré D, Clanet C. Water spring: a model for bouncing drops. *Europhys Lett*. 2003;62:237–243.
30. Richard D, Clanet C, Quéré D. Contact time of a bouncing drop. *Nature*. 2002;417:811.
31. Pasandideh-Fard M, Qiao YM, Chandra S, Mostaghimi J. Capillary effects during droplet impact on a solid surface. *Phys Fluids*. 1996; 8:650–659.
32. Mao T, Kuhn DCS, Tran H. Spread and rebound of liquid droplets upon impact on flat surfaces. *AIChE J*. 1997;43:2169–2179.
33. Park H, Carr WW, Zhu JY, Morris JF. Single drop impaction on a solid surface. *AIChE J*. 2003;49:2461–2471.
34. Roisman IV, Rioboo R, Tropea C. Normal impact of a liquid drop on a dry surface: model for spreading and receding. *Proc R Soc Lond A*. 2002;458:1411–1430.
35. van Dam DB, Le Clerc C. Experimental study of the impact of an ink-jet printed droplet on a solid substrate. *Phys Fluids*. 2004;16: 3403–3414.
36. Dong HM, Carr WW, Bucknal G. Temporally-resolved inkjet drop impaction on surfaces. *AIChE J*. 2007;53:2606–2617.
37. Son Y, Kim C, Yang DH, Ahn DJ. Spreading of an inkjet droplet on a solid surface with a controlled contact angle at low Weber and Reynolds numbers. *Langmuir*. 2008;24:2900–2907.
38. Oh J, Imai H, Hirashima H. Direct deposition of silica films using silicon alkoxide solution. *J Non-Cryst Solids*. 1998;241:91–97.
39. Qian BT, Shen ZQ. Fabrication of superhydrophobic surfaces by dislocation-selective chemical etching on aluminum, copper, and zinc substrates. *Langmuir*. 2005;21:9007–9009.
40. Bartolo D, Josserand C, Bonn D. Retraction dynamics of aqueous drops upon impact on non-wetting surfaces. *J Fluid Mech*. 2005; 545:329–338.
41. Bayer IS, Megaridis CM. Contact angle dynamics in droplets impacting on flat surfaces with different wetting characteristics. *J Fluid Mech*. 2006;558:415–449.
42. Zhang F, Zhang ZB, Geng J. Study on shrinkage characteristics of heated falling liquid films. *AIChE J*. 2005;51:2899–2907.
43. Alexeev A, Gambaryan-Roisman T, Stephan P. Marangoni convection and heat transfer in thin liquid films on heated walls with topography: experiments and numerical study. *Phys Fluids*. 2005;17: 062106.
44. Oron A, Davis SH, Bankoff SG. Long-scale evolution of thin liquid films. *Rev Mod Phys*. 1997;69:931–980.
45. Kataoka DE, Troian SM. A theoretical study of instabilities at the advancing front of thermally driven coating films. *J Colloid Interface Sci*. 1997;192:350–362.
46. Kataoka DE, Troian SM. Stabilizing the advancing front of thermally driven climbing films. *J Colloid Interface Sci*. 1998;203:335–344.
47. Brochard F. Motions of droplets on solid surfaces induced by chemical or thermal gradients. *Langmuir*. 1989;5:432–438.
48. de Gennes PG. Wetting: statics and dynamics. *Rev Mod Phys*. 1985; 57:827–842.
49. Callies M, Quéré D. On water repellency. *Soft Matter*. 2005;1:55–61.
50. Cassie ABD, Baxter S, Wettability of porous surface. *Trans Faraday Soc*. 1944;40:546–551.
51. Reyssat M, Pépin A, Marty F, Chen Y, Quéré D. Bouncing transitions on microtextured materials. *Europhys Lett*. 2006;74:306–312.

Manuscript received Jun. 22, 2008, and revision received Jan. 12, 2009.